# Kinetics of Elementary Reactions in the Chain Chlorination of Cyclopropane

**Michael D. Hurley,* William F. Schneider, Timothy J. Wallington, and David J. Mann†**

*Ford Research Laboratory, Mail Drop 3083/SRL, Dearborn, Michigan 48121-2053*

**John D. DeSain‡ and Craig A. Taatjes***

*Combustion Research Facility, Mail Stop 9055, Sandia National Laboratories, Livermore, California 94551-0969*

*Received: September 23, 2002; In Final Form: December 31, 2002*

The kinetics of elementary reactions involved in the chain chlorination of cyclopropane are examined using a combination of absolute and relative rate constant measurements and first principles electronic structure calculations. Relative rate methods are used in a smog chamber FTIR apparatus to determine $k(Cl + c\text{-}C_3H_6) = (1.15 \pm 0.17) \times 10^{-13}$ and $k(Cl + c\text{-}C_3H_5Cl) = (1.06 \pm 0.18) \times 10^{-12}$ cm$^3$ molecule$^{-1}$ s$^{-1}$ in 10−700 Torr of air, or $N_2$, diluent at 296 K. Absolute rate coefficients for the reaction of Cl with cyclopropane are measured between 293 and 623 K by a laser-photolysis/CW infrared absorption method. The data can be represented in Arrhenius form as $k(Cl + c\text{-}C_3H_6) = ((1.8 \pm 0.3) \times 10^{-10}$ cm$^3$ molecule$^{-1}$ s$^{-1}$)e$^{-(2150\pm100)/T}$. To support the experimental investigations, first principles electronic structure calculations are performed. Vibrational spectra of $c\text{-}C_3H_5Cl$, $c\text{-}C_3H_4Cl_2$, and $c\text{-}C_3H_3Cl_3$ are calculated and are presented. *gem*-$C_3H_4Cl_2$ is calculated to be the kinetically and thermodynamically most favored dichlorocyclopropane. The experimental observations are consistent with the computational findings.

## 1. Introduction

Optimization of the performance of modern internal combustion engines relies on computational models incorporating detailed descriptions of combustion chemistry.[1] Chemical models of combustion processes require accurate data concerning the formation and fate of alkyl radicals in such systems.[2] Reactions of chlorine atoms with suitable hydrocarbon precursors are often used as convenient sources of alkyl radicals for laboratory study. Prior to such studies it is advisable to understand the kinetics and mechanism of the Cl + hydrocarbon reaction. The cyclopropyl radical, as the smallest cyclic alkyl radical, is an interesting species for investigating the effects of ring strain energy on chemical reaction. In conjunction with a collaborative study[3] of the reaction of cyclopropyl radicals with $O_2$, we have studied the kinetics of the chain chlorination of cyclopropane.

In the present work a combination of absolute rate, relative rate, and first principles electronic structure calculations is employed to investigate elementary reactions in the chain chlorination of cyclopropane. Fundamental data concerning the kinetics, mechanisms, and thermochemistry of reactions 1 and 2 and the infrared spectra of $c\text{-}C_3H_5Cl$, $c\text{-}C_3H_4Cl_2$, and $c\text{-}C_3H_3Cl_3$ are reported herein.

$$Cl + c\text{-}C_3H_6 \rightarrow c\text{-}C_3H_5 + HCl \quad (1)$$

$$Cl + c\text{-}C_3H_5Cl \rightarrow c\text{-}C_3H_4Cl + HCl \quad (2)$$

## 2. Experiment

**2.1. FTIR Smog Chamber System at Ford Motor Company.** Experiments are performed in a 140-L Pyrex reactor interfaced to a Mattson Sirus 100 FTIR spectrometer described elsewhere.[4] The reactor is surrounded by 22 fluorescent black lamps (GE F15T8-BL) that are used to photochemically initiate the experiments. Cl atoms are generated by photolysis of molecular chlorine in 700 Torr total pressure of $N_2$ diluent at 295 ± 2 K. $c\text{-}C_3H_5Cl$ is produced by reaction 4.

$$Cl_2 + h\nu \rightarrow 2Cl \quad (3)$$

$$c\text{-}C_3H_5 + Cl_2 \rightarrow c\text{-}C_3H_5Cl + Cl \quad (4)$$

Loss of $c\text{-}C_3H_6$ and formation of products are monitored by Fourier transform infrared spectroscopy using an infrared path length of 27.5 m and a spectral resolution of 0.25 cm$^{-1}$. Infrared spectra are derived from 32 coadded interferograms. Reagents are obtained from commercial sources at the following stated purities (cyclopropane (>99.9%); chlorine (>99.99%); $N_2$ (UHP); $O_2$ (UHP)) and are used as received. In smog chamber experiments, unwanted loss of reactants and products via photolysis, dark chemistry, and wall reaction has to be considered. Control experiments are performed to check for these losses. Mixtures of $c\text{-}C_3H_6$ and air are subjected to UV irradiation for 5 min and then left in the dark for 30 min. There is no observable loss (<2%) of $c\text{-}C_3H_6$, $c\text{-}C_3H_5Cl$, or $c\text{-}C_3H_4Cl_2$ when mixtures containing these compounds are left in the chamber in the dark for 45 min. Heterogeneous reactions are not a significant complication in the present work.

**2.2. Theoretical Methods.** First principles electronic structure calculations are performed using the Mulliken[5] suite of programs. Heats of reaction, barrier heights, and bond energies are computed using a combined restricted open shell Hartree−Fock and second-order Møller−Plesset (MP2/ROHF) level of theory with a 6-311G** basis set. All structures are optimized at the ROHF level, and the energies at these geometries are corrected

* To whom correspondence should be addressed. E-mail: mhurley3@ford.com and cataatj@sandia.gov.

† Present address: Zyvex Corporation, 1321 N. Plano Road, Richardson, TX 75081.

‡ Present address: The Aerospace Corporation, 2350 E. El Segundo Blvd., El Segundo, CA 90245-4691.

10.1021/jp022121m CCC: $25.00 
Published on Web 03/04/2003

at the MP2 level. This level of theory has been applied to the reaction of Cl with methane, and excellent agreement is found with higher-level calculations performed by Dobbs and Dixon.[6] The MP2 optimized geometries for $CH_3^•$ and $CH_4$ they report are identical to those we obtained at the ROHF level, and the ROHF optimized internal coordinates for the $[CH_3\text{- -H- -Cl}]^•$ transition state agree to within 3% of their MP2 results. In addition, the ROHF optimized geometry of the cyclopropyl radical is in good overall agreement with the MP2/TZ2P optimized structure obtained elsewhere.[7] Finally, we computed and compared optimized structures for cyclopropane and chlorocyclopropane at both the ROHF and MP2 levels, using the same 6-311G** basis set, and the resulting internal coordinates agree to within 1%. Similar levels of theory have been applied successfully to other halogenated radical reactions.[8] ROHF is preferred over UHF, since for open-shell systems UHF has a tendency to produce errors that result from spin contamination of the HF wave function.[9] Unsuccessful attempts were made with density functional theory, using the B3LYP functional, to locate a transition state for the reaction of Cl with cyclopropane. The inability to locate a transition state or to underestimate barrier heights is a problem often encountered with density functional theory.[6,10,11] Vibrational spectra for the monochloro-, dichloro-, and trichlorocyclopropanes are computed at the ROHF level with harmonic frequencies scaled by the homogeneous scaling factor 0.9054.[12]

**2.3. Absolute Rate Coefficient Measurements at Sandia National Laboratories.** Absolute rate constants for the reaction $c\text{-}C_3H_6 + Cl$ are measured by using the laser-photolysis/CW infrared long path absorption (LP/CWIRLPA) method as described in previous publications.[13,14] The Cl is generated by excimer laser photolysis of $CF_2Cl_2$ at 193 nm, and the HCl product is detected by time-resolved infrared absorption of an F-center laser tuned to the R(8) line of the vibrational fundamental.

$$Cl_2 \xrightarrow{h\nu\ (355\ nm)} 2Cl \qquad (3)$$

$$Cl + c\text{-}C_3H_6 \rightarrow c\text{-}C_3H_5 + HCl \qquad (1)$$

The experiments are performed in a slow-flow reactor surrounded by a commercial ceramic-fiber heater. The IR probe is passed multiple times through the reactor using Herriott-type multipass optics.[15] This multipass arrangement allows the IR probe to intercept the UV photolysis beam only in the center of the flow cell, where the temperature is more readily controlled. The overall effective path length is approximately 20 m. To increase the signal-to-noise ratio, a balanced detector method is employed, with one detector (reference) monitoring the laser prior to the reactor and a second detector (signal) after multipassing through the flow cell. The total average dc power on each detector is kept equal, and the signals from the two detectors are subtracted to reduce laser amplitude noise.

The gases are admitted to the cell through calibrated mass flow controllers, and the total pressure in the cell is measured by a capacitance manometer and is actively controlled by a butterfly valve on the outlet. $CF_2Cl_2$ concentrations are $1.75 \times 10^{15}$ cm$^{-3}$, cyclopropane concentrations are varied from $2.6 \times 10^{15}$ to $14.2 \times 10^{15}$ cm$^{-3}$, and and Ar buffer (99.9999%) is added to reach a total density of $3.22 \times 10^{17}$ cm$^{-3}$. The cyclopropane has a manufacturer-stated purity of 99.9% (chromatographic lot analysis). Measurements of the impurity composition have been undertaken at Sandia National Laboratories by gas chromatographic analysis using flame ionization detection, and also by GC/MS. The major impurity is found to be 1,3-dichloropropane, with smaller amounts of 1,1-dichloropropane, 1-propanol, and propene. The contribution to the observed HCl formation of reaction of Cl with these impurities (at the 0.1% level) is significant at room temperature, amounting to ~20% of the measured rate constant, but decreases rapidly with increasing temperature as the Cl + cyclopropane rate coefficient increases.

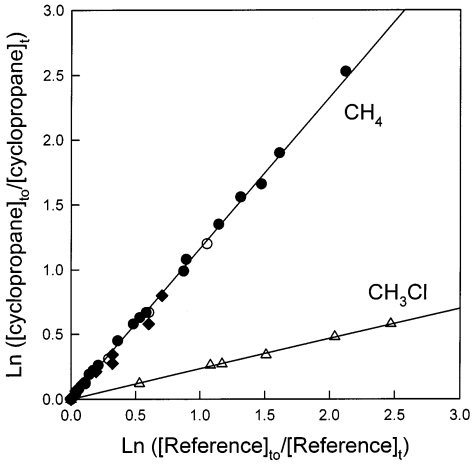


**Figure 1.** Loss of cyclopropane versus $CH_4$ (circles) and $CH_3Cl$ (triangles) following exposure to Cl atoms in 700 Torr of $N_2$ (open symbols) or air (filled symbols) diluent. Data acquired in 10 Torr of air are shown by filled diamonds.

## 3. Results and Discussion

**3.1. Relative Rate Study of $k(Cl + c\text{-}C_3H_6)$.** The kinetics of reaction 1 are measured relative to reactions 5 and 6 using the relative rate technique.[16]

$$Cl + c\text{-}C_3H_6 \rightarrow \text{products} \qquad (1)$$

$$Cl + CH_4 \rightarrow \text{products} \qquad (5)$$

$$Cl + CH_3Cl \rightarrow \text{products} \qquad (6)$$

Initial concentrations are 10−81 mTorr of $c\text{-}C_3H_6$, 10−15 mTorr of $CH_4$, 10 mTorr of $CH_3Cl$, and 104−657 mTorr of $Cl_2$ in 10 or 700 Torr of air or nitrogen diluent. The observed loss of $c\text{-}C_3H_6$ versus the loss of the reference compounds in the presence of Cl atoms is shown in Figure 1. As seen from Figure 1, there is no discernible effect of the nature or total pressure of diluent gas. Linear least-squares analysis of the data in Figure 1 gives $k_1/k_5 = 1.17 \pm 0.09$ and $k_1/k_6 = 0.233 \pm 0.014$. We derive $k_1 = (1.17 \pm 0.09) \times 10^{-13}$ using $k_5 = 1.0 \times 10^{-13}$,[17] and $k_1 = (1.12 \pm 0.07) \times 10^{-13}$ using $k_6 = 4.80 \times 10^{-13}$ cm$^3$ molecule$^{-1}$ s$^{-1}$.[17] We estimate that potential systematic errors associated with uncertainties in the reference rate constants add 10% to the uncertainty range for $k_1$. Propagating this additional uncertainty for the two relative rate measurements gives $k_1 = (1.17 \pm 0.15) \times 10^{-13}$ and $k_1 = (1.12 \pm 0.13) \times 10^{-13}$ cm$^3$ molecule$^{-1}$ s$^{-1}$. We choose to quote a final value for $k_1$ which is the average with error limits which encompass the extremes of the individual determinations; hence, $k_1 = (1.15 \pm 0.17) \times 10^{-13}$ cm$^3$ molecule$^{-1}$ s$^{-1}$. This result is in good agreement with the previous absolute rate measurement of $k_1 = (1.21 \pm 0.15) \times 10^{-13}$ by Baghal-Vayjooee and Benson[18] but lower than $k_1 = 1.7 \times 10^{-13}$ cm$^3$ molecule$^{-1}$ s$^{-1}$ from the relative rate study by Knox and Nelson[19] (based upon $k(Cl + C_2H_6) = 5.7 \times 10^{-11}$ cm$^3$ molecule$^{-1}$ s$^{-1}$ at 298 K[17]). Knox and Nelson reported an

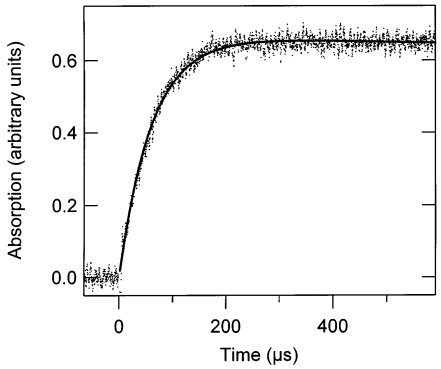


**Figure 2.** Time-resolved absorption trace of HCl formed in the reaction of Cl with cyclopropane at 423 K. The solid line shows a fit to the difference of two exponentials. The cyclopropane concentration is 1.42 × $10^{16}$ $cm^{-3}$.

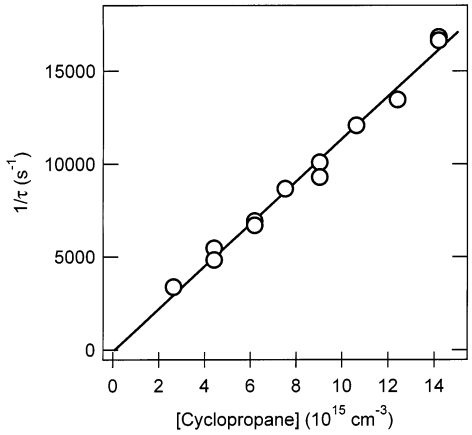


**Figure 3.** Plot of the pseudo-first-order rate coefficient for HCl formation versus cyclopropane concentration at 423 K. The slope of this plot yields the second-order rate coefficient for the Cl + cyclopropane reaction.

appreciable dark reaction between $Cl_2$ and cyclopropane in their system that may explain an overestimation of $k_1$ in their work.

**3.2. Absolute Rate Coefficients for Cl + *c*-$C_3H_6$.** A typical time-resolved absorption signal from formation of HCl in the Cl + cyclopropane reaction is shown in Figure 2. This signal can be fit by the difference of two exponentials,[20] with the rise time reflecting the formation of HCl by the Cl + cyclopropane reaction and the decay reflecting loss of HCl, principally by diffusion out of the probe region. A plot of the reciprocal of the rise time versus cyclopropane concentration, as shown in Figure 3, yields a linear plot, the slope of which provides an absolute measurement of the second-order rate coefficient. The intercept of this plot reflects other losses of Cl atom, including diffusion and possible reactions with impurities in the photolyte or buffer gas.[20] The absolute rate coefficients for Cl + cyclopropane measured by LP/CWIRLPA are given in Table 1 and shown in Figure 4. The error estimates are $\pm 2\sigma$ on the basis of the statistical error of the rate coefficient determination convolved with an estimate of the uncertainties associated with concentration, temperature, and pressure measurements. The absolute measurement is expected to suffer a systematic error associated with the impurities in the cyclopropane sample. This contribution can be estimated on the basis of the impurity composition from the gas chromatographic analysis. The relative peak areas for the 1,3-dichloropropane, 1,1-dichloropropane, 1-propanol, and propene impurities, using flame ionization detection, are 71:13:10:6. The room-temperature rate coefficients for the Cl + 1,3-dichloropropane,[21] Cl + propene,[22,23] and Cl + 1-propanol[24−26] reactions have been measured. The Cl + 1,1-dichloropropane rate coefficient is set to the value for the Cl + 1-chloropropane reaction.[21,27,28] Assuming a total impurity level of 0.1% (the upper limit based on the manufacturer's lot analysis), the rate coefficient from impurity reactions is estimated to be 3.7 × $10^{-14}$ $cm^3$ $molecule^{-1}$ $s^{-1}$. Comparison of the room-temperature absolute measurement with the relative rate measurements, which are insensitive to impurities in the cyclopropane sample, yields a difference of 3.4 × $10^{-14}$ $cm^3$ $molecule^{-1}$ $s^{-1}$.

**TABLE 1: Measured Absolute Rate Coefficients for Cl + Cyclopropane**

| temp (K) | $k_{meas}$ ($cm^3$ $molecule^{-1}$ $s^{-1}$) | $k_{corr}$[a] ($cm^3$ $molecule^{-1}$ $s^{-1}$) |
|---|---|---|
| 293 | (1.49 ± 0.12) × $10^{-13}$ | (1.12 ± 0.22) × $10^{-13}$ |
| 373 | (5.67 ± 0.44) × $10^{-13}$ | (5.30 ± 0.54) × $10^{-13}$ |
| 423 | (1.09 ± 0.06) × $10^{-12}$ | (1.04 ± 0.07) × $10^{-12}$ |
| 473 | (1.92 ± 0.08) × $10^{-12}$ | (1.88 ± 0.09) × $10^{-12}$ |
| 523 | (2.81 ± 0.12) × $10^{-12}$ | (2.77 ± 0.13) × $10^{-12}$ |
| 573 | (4.13 ± 0.18) × $10^{-12}$ | (4.09 ± 0.19) × $10^{-12}$ |
| 623 | (5.75 ± 0.36) × $10^{-12}$ | (5.71 ± 0.37) × $10^{-12}$ |

[a] Includes correction for estimated impurity contribution of 3.7 × $10^{-14}$ $cm^3$ $molecule^{-1}$ $s^{-1}$ and additional uncertainty estimate of 1 × $10^{-14}$ $cm^3$ $molecule^{-1}$ $s^{-1}$.

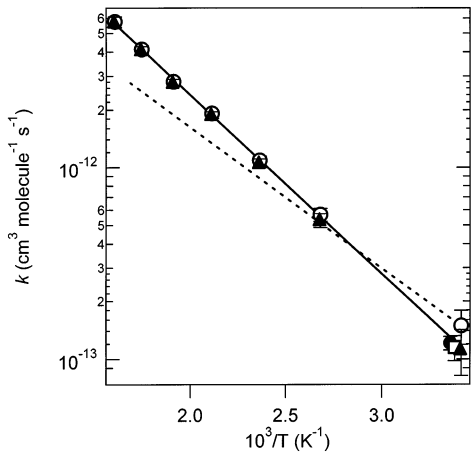


**Figure 4.** Arrhenius plot of the measured rate coefficients for the Cl + cyclopropane reaction. The present absolute measurements are shown as the open circles and the solid triangles (corrected for estimated impurity contributions). The present relative rate determination is shown as the open square. The absolute measurement by Baghal-Vayjooee and Benson[18] is given as the solid circle, and the Arrhenius fit from the relative measurements of Knox and Nelson[19] (using $k_{Cl+ethane}$ from ref 13) is shown as the dashed line. The solid line is a weighted fit to the present data, $k_2 = ((1.8 \pm 0.3) \times 10^{-10}$ $cm^3$ $molecule^{-1}$ $s^{-1})e^{-(2150\pm100)/T}$.

On the basis of measurements of similar Cl + hydrocarbon[13,23] and Cl + alcohol[20,26] reactions, the Cl + impurity reactions are unlikely to have a significant temperature dependence. The correction for impurity contributions therefore becomes insignificant at higher temperatures, where the Cl + cyclopropane rate coefficient is larger. Rate coefficients corrected for the estimated impurity contribution ($k_{corr} = k_{obs} -$ 3.7 × $10^{-14}$ $cm^3$ $molecule^{-1}$ $s^{-1}$) are shown as the triangles in Figure 4. The temperature-dependent absolute rate coefficient measurements can be fit to an Arrhenius form, shown as the straight line in Figure 4, $k_1 = ((1.8 \pm 0.3) \times 10^{-10}$ $cm^3$ $molecule^{-1}$ $s^{-1})e^{-(2150\pm100)/T}$. A weighted fit to the uncorrected absolute measurements and the present relative rate measurement gives a result essentially identical to that from a fit to the corrected absolute determinations ($k_{corr}$). The activation energy is in excellent agreement with the 4.14 kcal $mol^{-1}$ activation

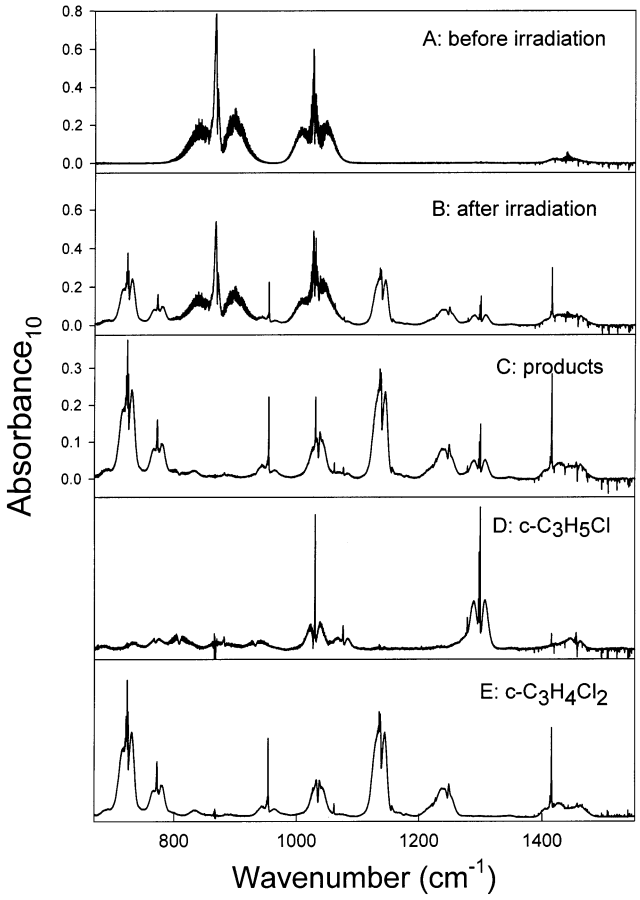


**Figure 5.** IR spectra acquired before (A) and after (B) a 10 s UV irradiation of a mixture of 99.2 mTorr of cyclopropane and 1 Torr of $Cl_2$ in 700 Torr of $N_2$ diluent. Subtraction of cyclopropane features from panel B gives panel C. Spectra of *c*-$C_3H_5Cl$ and *c*-$C_3H_4Cl_2$ are shown in panels D and E.

energy reported in the previous measurement of the temperature dependence by Knox and Nelson.[19] However, using the most recent measurement of the temperature dependence of the Cl + ethane reaction to place the Knox and Nelson relative rate measurements on an absolute scale yields somewhat poorer agreement, as shown by the dashed line in Figure 4.

**3.3. Photochemical Chain Chlorination of *c*-$C_3H_6$.** The chlorination of cyclopropane is studied using the UV irradiation of *c*-$C_3H_6/Cl_2/N_2$ mixtures. The reactions occurring in such a chemical system are

$$Cl_2 + h\nu \rightarrow 2Cl \quad (3)$$

$$c\text{-}C_3H_6 + Cl \rightarrow c\text{-}C_3H_5 + HCl \quad (1)$$

$$c\text{-}C_3H_5 + Cl_2 \rightarrow c\text{-}C_3H_5Cl + Cl \quad (4)$$

$$c\text{-}C_3H_5Cl + Cl \rightarrow c\text{-}C_3H_4Cl + HCl \quad (2)$$

$$c\text{-}C_3H_4Cl + Cl_2 \rightarrow c\text{-}C_3H_4Cl_2 + Cl \quad (7)$$

$$c\text{-}C_3H_4Cl_2 + Cl \rightarrow c\text{-}C_3H_3Cl_2 + HCl \quad (8)$$

$$c\text{-}C_3H_3Cl_2 + Cl_2 \rightarrow c\text{-}C_3H_3Cl_3 + Cl \quad (9)$$

The chain is terminated by loss of Cl atoms through recombination, reaction with other radicals, or loss at the walls. Initial concentrations are 48−207 mTorr of *c*-$C_3H_6$ and 100−1040 mTorr of $Cl_2$ in 700 Torr of $N_2$ diluent at 296 ± 3 K. Short irradiations (1−2 s) resulted in the loss of cyclopropane and the formation of a product with prominent IR features at 1031 and 1300 $cm^{-1}$. Further irradiation lead to the formation of a new set of product features at 735, 772, 954, 1035, 1137, 1249, and 1415 $cm^{-1}$ which scaled linearly in all spectra and which increased at the expense of the original product. It seems reasonable to assign the first set of features to chlorocyclopropane formed in reaction 4 and the second set of features to dichloropropane formed in reaction 7. Figure 5 shows infrared spectra acquired before (A) and after (B) a 10 s irradiation of 99.2 mTorr of *c*-$C_3H_6$ and 1.0 Torr of $Cl_2$ in 700 Torr of $N_2$. The 10 s irradiation led to 32% consumption of *c*-$C_3H_6$. Subtraction of features attributable to *c*-$C_3H_6$ from panel B gives the product spectrum shown in panel C. By comparing product spectra containing different amounts of chloro- and dichlorocyclopropane, we are able to provide the IR spectra of *c*-$C_3H_5$-Cl and *c*-$C_3H_4Cl_2$ shown in panels D and E. For experiments employing cyclopropane conversions of <90%, only two products are observed: *c*-$C_3H_5Cl$ and *c*-$C_3H_4Cl_2$. Absolute calibration of the *c*-$C_3H_5Cl$ and *c*-$C_3H_4Cl_2$ spectra is achieved by comparing the results from experiments with different consumptions of cyclopropane and different relative amounts of *c*-$C_3H_5Cl$ and *c*-$C_3H_4Cl_2$ and equating the sum of *c*-$C_3H_5Cl$ and *c*-$C_3H_4Cl_2$ with the cyclopropane loss. This approach gave $\sigma_e$(*c*-$C_3H_5Cl$) at 1307 $cm^{-1}$ = (1.62 ± 0.32) × $10^{-19}$ and $\sigma_e$-(*c*-$C_3H_4Cl_2$) at 1145 $cm^{-1}$ = (2.55 ± 0.51) × $10^{-19}$ $cm^2$ $molecule^{-1}$.

There are three possible dichlorocyclopropane products: *gem*-$C_3H_4Cl_2$ (both Cl atoms attached to the same C atom), *trans*-1,2-$C_3H_4Cl_2$ (Cl atoms attached to different C atoms and directed to opposite sides of the planar ring), and *cis*-1,2-$C_3H_4Cl_2$ (similar to *trans*-$C_3H_4Cl_2$ except both Cl atoms are on the same face of the planar ring):

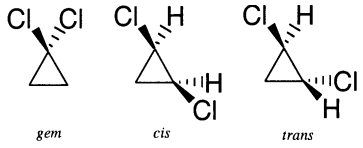


As discussed in section 3.6, the *gem*-isomer is kinetically and thermodynamically favored and we assign the spectrum in Figure 5E to *gem*-$C_3H_4Cl_2$. Continued irradiation of $C_3H_4Cl_2/Cl_2/N_2$ mixtures led to the loss of $C_3H_4Cl_2$ and the formation of another product with IR features at 700, 855, 900, 955, 1030, 1045, 1065, and 1405 $cm^{-1}$ which we ascribe to $C_3H_3Cl_3$. As is the case for the possible $C_3H_4Cl_2$ products, three isomers of $C_3H_3Cl_3$ are possible, and we use a similar nomenclature to define them as *gem* (two Cl atoms on one C and one Cl on another C), *cis* (Cl atoms on all three C atoms, all on the same side of the $C_3$ ring), or *trans* (Cl atoms on all three C atoms, one on the opposite face of the $C_3$ ring from the other two):

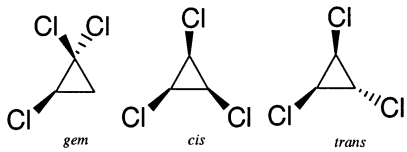


**3.4. Relative Rate Study of *k*(Cl + *c*-$C_3H_5Cl$).** Irradiation of *c*-$C_3H_6/Cl_2/N_2$ mixtures results in the conversion of *c*-$C_3H_6$ into *c*-$C_3H_5Cl$ that is then converted into *c*-$C_3H_4Cl_2$. The yield of *c*-$C_3H_5Cl$ is described by the following expression[29]

$$\frac{[c\text{-}C_3H_5Cl]}{[c\text{-}C_3H_6]_0} = \left\{\frac{1}{(1 - k_2/k_1)}\right\}(1 - x)\{(1 - x)^{(k_2/k_1)-1} - 1\}$$

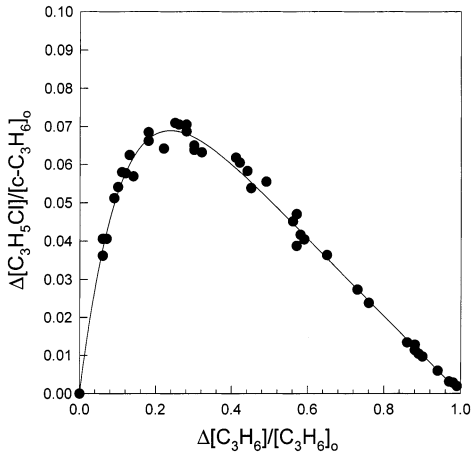


**Figure 6.** Concentration of *c*-$C_3H_5Cl$ normalized to the initial concentration of *c*-$C_3H_6$ versus the fractional consumption of *c*-$C_3H_6$ following irradiation of *c*-$C_3H_6/Cl_2/N_2$ mixtures. The curve is a fit to the data (see text for details).

where $x$ is the conversion of cyclopropane, defined as

$$x \equiv \frac{\Delta[c\text{-}C_3H_6]}{[c\text{-}C_3H_6]_0}$$

Figure 6 shows a plot of $([c\text{-}C_3H_5Cl]_t/[c\text{-}C_3H_5Cl]_0)$ versus $\Delta[c\text{-}C_3H_6]/[c\text{-}C_3H_6]_0$ for the chlorination experiments described above. The curve in Figure 6 shows the result of a least-squares fit of the expression above to the data which gives $k_2/k_1 = 9.2 \pm 0.7$. Combining this ratio with the value for $k_1$ reported in section 3.1 gives $k_2 = (1.06 \pm 0.18) \times 10^{-12}$ cm$^3$ molecule$^{-1}$ s$^{-1}$.

**3.5. Computational Study of Hydrogen Abstraction.** The objective of this computational study is to investigate the kinetics and mechanism of the reaction of Cl atoms with cyclopropane and determine which of the dichloro- and trichlorocyclopropane isomers are predominant products using first principles electronic structure theory.

The rate-limiting step for the reaction of chlorine with cyclopropane is the hydrogen atom abstraction step leading to the formation of a cyclopropyl radical (reaction 1). As computed at the ROHF level, this reaction proceeds with a barrier of 25.6 kcal mol$^{-1}$ with respect to the energy of the reactants at infinite separation. Structures for cyclopropane and the transition state for this reaction are shown in Figure 7. The transition state structure for Cl + cyclopropane is almost identical to that of the reaction of Cl with methane. For the chlorination of methane the ROHF transition state internal coordinates $r_{CH_a}$ and $r_{H_aCl}$ have the values 1.309 and 1.517 Å, respectively, where $H_a$ corresponds to the abstracted H atom. Similarly, the transition state internal coordinates $r_{CH_a}$ and $r_{H_aCl}$ for the cyclopropane transition state have the values 1.312 and 1.503 Å, respectively. The C−$H_a$−Cl angle in the methane transition state is 180°,[6] as is expected because of the 3-fold symmetry along the reaction coordinate. This angle is slightly perturbed by 1.9° in the cyclopropane transition state as a result of van der Waals interactions with nearby H atoms. Since Hartree−Fock notoriously overestimates barrier heights,[30] which will erroneously underestimate rate constants, the energies are corrected with MP2 using the ROHF geometries. The MP2 energy correction lowers the barrier to 8.3 kcal mol$^{-1}$.

The prefactor, $A$, and transition state theory (TST)[31] rate constant, $k_{TST}$, for this reaction are also computed at 300 K using the ROHF vibrational frequencies and moments of inertia. The

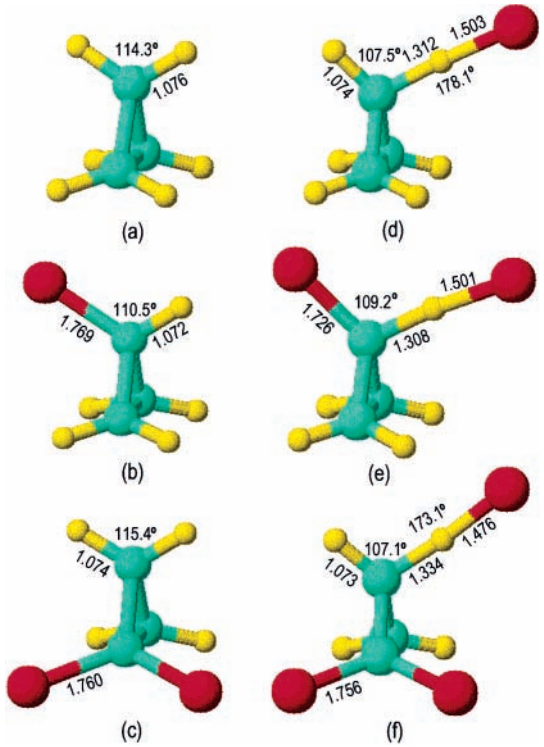


**Figure 7.** ROHF/6-311G** optimized structures for (a) $C_3H_6$, (b) $C_3H_5Cl$, (c) *gem*-$C_3H_4Cl_2$, (d) the transition state for $C_3H_6 + Cl^\bullet \rightarrow C_3H_5^\bullet + HCl$, (e) the transition state for $C_3H_5Cl + Cl^\bullet \rightarrow$ *gem*-$C_3H_4Cl^\bullet + HCl$, and (f) the transition state for *gem*-$C_3H_4Cl_2 + Cl^\bullet \rightarrow$ *gem*-$C_3H_3Cl_2^\bullet + HCl$.

vibrational frequencies are scaled using the homogeneous scaling factor 0.9054.[10] The prefactor and rate constant are listed in Table 2 along with the MP2/ROHF heat of reaction, barrier height, and zero-point energy corrected barrier height. The TST rate constant is calculated using the zero-point corrected MP2/ROHF barrier height, $\Delta E^{\ddagger}_{ZPE}$, 4.0 kcal mol$^{-1}$, using the expression

$$k_{TST} = \sigma N_A \frac{k_B T}{h} \frac{Q^{TS}}{Q_A Q_B} \exp\left(\frac{-\Delta E^{\ddagger}_{ZPE}}{k_B T}\right) = A \exp\left(\frac{-\Delta E^{\ddagger}_{ZPE}}{k_B T}\right)$$

where $Q_A$ and $Q_B$ are the partition functions for the reactants and $Q^{TS}$ is the transition state partition function. The symmetry factor $\sigma$ represents the number of identical reaction pathways and equals 6 for the reaction of Cl with cyclopropane. The TST calculated rate constant $5 \times 10^{-14}$ cm$^3$ molecule$^{-1}$ s$^{-1}$ (Table 2) underestimates the experimental value by only a factor of 2, which is remarkable agreement for the crude computational model applied here. This agreement gives confidence that the calculated barriers can be used to assess the relative rates of hydrogen abstraction from the Cl-substituted cyclopropanes.

The C−H bond dissociation energy (BDE) is one possible indicator of the relative ease of H abstraction by Cl atoms. A reasonable estimate of the $C_3H_5$−H BDE can be obtained from the isodesmic[32,33] reaction

$$c\text{-}C_3H_6 + CH_3^\bullet \rightarrow c\text{-}C_3H_5^\bullet + CH_4 \qquad (10)$$

in conjunction with the experimental heat of reaction of 105.1 kcal mol$^{-1}$ for $CH_4 \rightarrow CH_3^\bullet + H^\bullet$.[34] Isodesmic reactions are those in which reactants and products contain the same type and number of bonds.[32,33] Because of this electronic similarity, errors in the energy due to defects in the basis set and electronic

**TABLE 2: MP2/6-311G**//ROHF/6-311G** Barrier Heights ($\Delta E^{\ddagger}$), Zero-Point Energy Corrected Barrier Heights ($\Delta E^{\ddagger}_{ZPE}$), Transition State Theory Prefactors ($A$), and Transition State Theory Rate Constants ($k_{TST}$)**

| reaction | $\Delta E^{\ddagger}$ [a] | $\Delta E^{\ddagger}_{ZPE}$ [a] | $A$ [b,c] | $k_{TST}$ [b,c] |
|---|---|---|---|---|
| $C_3H_6 + Cl^{\bullet} \rightarrow C_3H_5^{\bullet} + HCl$ | 8.3 | 4.0 | $3.7 \times 10^{-11}$ | $4.6 \times 10^{-14}$ |
| $C_3H_5Cl + Cl^{\bullet} \rightarrow$ *gem*-$C_3H_4Cl^{\bullet} + HCl$ | 6.0 | 1.8 | $2.0 \times 10^{-11}$ | $1.0 \times 10^{-13}$ |
| $C_3H_5Cl + Cl^{\bullet} \rightarrow$ *trans*-$C_3H_4Cl^{\bullet} + HCl$ | 9.6 | 5.1 | $4.3 \times 10^{-11}$ | $8.3 \times 10^{-15}$ |
| $C_3H_5Cl + Cl^{\bullet} \rightarrow$ *cis*-$C_3H_4Cl^{\bullet} + HCl$ | 12.1 | 7.6 | $2.7 \times 10^{-11}$ | $7.6 \times 10^{-17}$ |
| *gem*-$C_3H_4Cl_2 + Cl^{\bullet} \rightarrow$ *gem*-$C_3H_3Cl_2^{\bullet} + HCl$ | 12.3 | 7.7 | $1.2 \times 10^{-11}$ | $2.8 \times 10^{-17}$ |
| *trans*-$C_3H_4Cl_2 + Cl^{\bullet} \rightarrow$ *gem*-$C_3H_3Cl_2^{\bullet} + HCl$ | 9.2 | 4.9 | $2.8 \times 10^{-12}$ | $7.6 \times 10^{-16}$ |
| *trans*-$C_3H_4Cl_2 + Cl^{\bullet} \rightarrow$ *trans*-$C_3H_3Cl_2^{\bullet} + HCl$ | 12.9 | 8.4 | $4.0 \times 10^{-12}$ | $2.0 \times 10^{-16}$ |
| *cis*-$C_3H_4Cl_2 + Cl^{\bullet} \rightarrow$ *gem*-$C_3H_3Cl_2^{\bullet} + HCl$ | 5.7 | 1.4 | $4.6 \times 10^{-12}$ | $3.3 \times 10^{-18}$ |
| *cis*-$C_3H_4Cl_2 + Cl^{\bullet} \rightarrow$ *trans*-$C_3H_3Cl_2^{\bullet} + HCl$ | 9.9 | 5.3 | $3.3 \times 10^{-12}$ | $4.3 \times 10^{-16}$ |
| *cis*-$C_3H_4Cl_2 + Cl^{\bullet} \rightarrow$ *cis*-$C_3H_3Cl_2^{\bullet} + HCl$ | 14.7 | 10.2 | $2.3 \times 10^{-12}$ | $1.7 \times 10^{-19}$ |

[a] Energies in kcal mol$^{-1}$. [b] $k$ in cm$^3$ molecule$^{-1}$ s$^{-1}$. [c] Prefactors and rate constants computed at 300 K.

**TABLE 3: MP2/6-311G**//ROHF/6-311G** C−H Bond Energies and Carbon Radical Spin Densities**

| reaction | BDE[a] | C spin density |
|---|---|---|
| $C_3H_6 \rightarrow C_3H_5^{\bullet} + H^{\bullet}$ | 102.1 | 0.9316 |
| $C_3H_5Cl \rightarrow$ *gem*-$C_3H_4Cl^{\bullet} + H^{\bullet}$ | 99.7 | 0.8776 |
| $C_3H_5Cl \rightarrow$ *trans*-$C_3H_4Cl^{\bullet} + H^{\bullet}$ | 102.2 | 0.9202 |
| $C_3H_5Cl \rightarrow$ *cis*-$C_3H_4Cl^{\bullet} + H^{\bullet}$ | 103.3 | 0.9314 |
| *gem*-$C_3H_4Cl_2 \rightarrow$ *gem*-$C_3H_3Cl_2^{\bullet} + H^{\bullet}$ | 103.3 | 0.9228 |
| *trans*-$C_3H_4Cl_2 \rightarrow$ *gem*-$C_3H_3Cl_2^{\bullet} + H^{\bullet}$ | 101.0 | 0.8804 |
| *trans*-$C_3H_4Cl_2 \rightarrow$ *trans*-$C_3H_3Cl_2^{\bullet} + H^{\bullet}$ | 103.4 | 0.9193 |
| *cis*-$C_3H_4Cl_2 \rightarrow$ *gem*-$C_3H_3Cl_2^{\bullet} + H^{\bullet}$ | 98.4 | 0.8695 |
| *cis*-$C_3H_4Cl_2 \rightarrow$ *trans*-$C_3H_3Cl_2^{\bullet} + H^{\bullet}$ | 101.7 | 0.9055 |
| *cis*-$C_3H_4Cl_2 \rightarrow$ *cis*-$C_3H_3Cl_2^{\bullet} + H^{\bullet}$ | 104.0 | 0.9296 |

[a] Zero-point corrected bond dissociation energies calculated from the isodesmic reaction $C_3H_{6-n}Cl_n + CH_3^{\bullet} \rightarrow C_3H_{5-n}Cl_n^{\bullet} + CH_4$ using the experimental bond dissociation energy of 105.1 kcal mol$^{-1}$ for $CH_4 \rightarrow CH_3^{\bullet} + H^{\bullet}$.[34]

correlation tend to cancel between reactants and products. The $C_3H_5$−H BDE derived from reaction 10 using the MP2 and ZPE corrected energies is 102.1 kcal mol$^{-1}$ (Table 3), or 4.2 kcal mol$^{-1}$ less than that derived from the reaction 1 equilibrium.[18]

Chlorination of the cyclopropyl radical produces chlorocyclopropane (reaction 4), and the calculated scaled vibrational spectrum agrees well with the experimentally observed spectrum (Figure 5D). As described above, further chlorination can produce up to three possible dichlorocyclopropane isomers. The calculated vibrational spectra for each of these three were compared with the observed spectrum of the dichlorocyclopropane product (Figure 5E). The most intense peaks in the calculated spectra for the *gem*, *trans*, and *cis* isomers are located at 1145, 666, and 1330 cm$^{-1}$, respectively, compared to the most intense peak at 1140 cm$^{-1}$ in the experimental spectrum. The bands at 666 and 1330 cm$^{-1}$ expected for the *trans* and *cis* isomer spectra do not appear in the experimental spectrum. Furthermore, an intense peak in the experimental spectrum at 725 cm$^{-1}$ is consistent with the asymmetric C−Cl stretch in the *gem* isomer that is not present in the *trans* or *cis* isomers. These results provide strong evidence that chlorination of chlorocyclopropane proceeds predominately or exclusively to the *gem*-dichlorocyclopropane product. Vibrational frequencies and relative intensities for the *gem* isomer are listed in Table 4 along with the experimental frequencies for dichlorocyclopropane. Intensities are uniformly scaled such that the most intense peak has a value of 100.

To explain this preference, MP2/ROHF bond dissociation energies (BDEs) and barrier heights are computed for the three reactions leading to *gem*, *trans*, and *cis*-chlorocyclopropyl radical intermediates and are listed in Tables 2 and 3. The C−H BDE leading to the *gem* radical is lower than that leading to *trans* and *cis* radicals by 2−3 kcal mol$^{-1}$. The zero-point energy corrected barrier leading to the *gem* radical intermediate is also more than 3 kcal mol$^{-1}$ lower than the barrier leading to the *trans* radical and almost 6 kcal mol$^{-1}$ lower than that leading to the *cis* radical, consistent with the BDEs. In the *gem* radical unpaired electron density can be delocalized from the C center to the Cl atom, stabilizing this radical relative to the other two isomers. This greater delocalization is reflected in a lower electron spin density on the C center, as shown in Table 3.

The structures of chlorocyclopropane and the transition state leading to the *gem* radical intermediate are shown in Figure 7. Also listed in Table 2 are prefactors and rate constants for each of the three possible reactions computed at 300 K. A somewhat surprising result is the order of magnitude larger prefactors for the *trans* and *cis* reactions over the *gem* reaction. This is partially a result of the statistical advantage of forming the *trans* and *cis* intermediates over the *gem* intermediate. There exist two equivalent pathways leading to each of the *trans* and *cis* radicals as opposed to just a single pathway leading directly to the *gem* radical. Since the prefactor is a measure of the encounter rate, this suggests that the *gem* pathway is only energetically favored over the remaining two pathways, even though encounters leading to the *trans* and *cis* pathways occur more frequently. The computed rate constant for the *gem* pathway is a factor of 2 greater than $k_{TST}$ for H abstraction from $C_3H_6$ (Table 2), in good qualitative agreement with the factor of 9 derived from the relative rate study above.

The above argument is based on the notion that, once formed, the *gem* radical only reacts with $Cl_2$ to produce the *gem* product (reaction 7). Internal isomerization of the *gem* radical to the *trans* by H migration is possible but the MP2/ROHF barrier of 49.0 kcal mol$^{-1}$ indicates that this is a very unlikely pathway. The barrier for a direct *gem* → *cis* radical isomerization is expected to be even higher because of the very large strain involved. Another possibility is ring-opening of the *gem* radical to form a chlorinated allyl radical. Although ring-opening was not explicitly investigated in this study, conclusions regarding its occurrence can be drawn from previous studies of the ring-opening of the cyclopropyl radical.[35−38] Both experimental[35,36] and high-level computational[37,38] studies predict a barrier of 22 kcal/mol for ring-fission leading to the allyl radical. This is still substantially larger than the zero-point corrected barriers for H atom abstraction, and therefore, ring-opening is not expected under the experimental conditions reported in this study.

A similar approach was used to examine the three possible trichlorocyclopropane isomers. The most intense peaks in the calculated vibrational spectra for the *gem*-, *trans*-, and *cis*-trichlorocyclopropane isomers are located at 766, 651, and 686 cm$^{-1}$, respectively, compared to the most intense peak in the experimental spectra at 785 cm$^{-1}$. The second most intense peaks in the calculated spectra for the *gem*, *trans*, and *cis* isomers are located at 1074, 1236, and 1365 cm$^{-1}$, respectively,

**TABLE 4: Scaled ROHF/6-311G** Normal-Mode Frequencies and IR Intensities**

| *gem*-$C_3H_4Cl_2$ | | | *gem*-$C_3H_3Cl_3$ | | |
|---|---|---|---|---|---|
| mode description | freq[a] theory (expt) | rel int[b] | mode description | freq[a] theory (expt) | rel int[b] |
| Cl−C−Cl wag | 270 | 1 | Cl−C−C−Cl torsion | 146 | 2 |
| sym Cl−C−Cl def | 292 | 0 | Cl−C−C−Cl torsion | 168 | 2 |
| Cl−C−C def | 297 | 0 | Cl−C−Cl def | 264 | 2 |
| Cl−C−C def | 394 | 0 | Cl−C−C def | 299 | 1 |
| sym C−Cl str | 482 | 25 | Cl−C−C def | 393 | 2 |
| asym C−Cl str | 715 (725) | 92 | sym C−Cl str | 449 | 4 |
| asym $CH_2$ rock | 763 (775) | 28 | | 515 | 24 |
| asym $CH_2$ wag | 886 | 1 | | 675 | 37 |
| asym C−C−C def | 933 | 0 | $CH_2$ rock | 766 (700) | 100 |
| sym C−C−C def | 971 (960) | 21 | $CH_2$ wag | 914 (855) | 17 |
| sym $CH_2$ rock | 1076 (1025) | 13 | | 962 (900) | 4 |
| sym H−C−C def | 1099 | 1 | | 980 (955) | 9 |
| sym H−C−C def | 1145 (1140) | 100 | H−C−C def | 1074 (1030) | 41 |
| asym H−C−C def | 1160 | 0 | H−C−C def | 1104 (1045) | 11 |
| sym $CH_2$ def | 1240 (1240) | 19 | H−C−C def | 1135 (1065) | 30 |
| asym $CH_2$ def | 1431 | 9 | H−C−C def | 1233 | 14 |
| sym C−C str | 1477 (1420) | 7 | sym $CH_2$ def | 1326 | 17 |
| asym C−H str | 2976 | 9 | sym C−C str | 1451 (1405) | 14 |
| sym C−H str | 2981 | 1 | asym C−H str | 2978 | 1 |
| sym C−H str | 3057 | 0 | asym C−H str | 3050 | 4 |
| asym C−H str | 3067 | 4 | sym C−H str | 3067 | 1 |

[a] Frequencies in units of $cm^{-1}$. [b] Relative intensities scaled to 100 for the most intense mode.

compared to the second most intense peak in the experimental spectra at 1030 $cm^{-1}$. The similarity between the calculated spectra for *gem*-$C_3H_3Cl_3$ and the experimental spectra suggests that the *gem* isomer is the only observed trichlorocyclopropane product. Calculated frequencies and assignments for *gem*-$C_3H_3Cl_3$ are listed in Table 4 along with the experimental frequencies.

From the results above, the only experimentally relevant H abstraction pathway (reaction 8) starts from *gem*-$C_3H_4Cl_2$, and as all the H atoms are equivalent in this molecule, only one abstraction pathway is possible. As shown in Table 2, the reaction barrier and rate constant for this reaction are consistent with the *cis* and *trans* results for $C_3H_5Cl$, as are the C−H BDE and C center spin density. H abstraction and, thus, *gem*-trichlorocyclopropane formation are predicted to occur much more slowly than mono- and dichlorocyclopropane formation. H abstraction is predicted to be more rapid from the *cis*- and *trans*-dichlorocyclopropane isomers (Table 2); we see that the H abstraction barrier is predominantly determined by the presence or absence of a Cl atom at the reacting C center and that the reaction barrier scales with the calculated C−H BDE and with the C center spin density in the daughter radical.

In summary, the computational results are consistent with a model in which *gem*-$C_3H_4Cl_2$ is the predominant product of chlorination of $C_3H_5Cl$, and *gem*-$C_3H_3Cl_3$ is the only product of chlorination of *gem*-$C_3H_4Cl_2$. Both chlorinations occur by H abstraction and chlorine substitution with preservation of the radical stereochemistry.

## 4. Conclusion

A large self-consistent body of experimental and computational data concerning the reactions important in the photochemical chain chlorination of cyclopropane is presented. Chlorination is initiated by reaction of Cl atoms with cyclopropane, which proceeds with a rate constant $k_1 = ((1.8 \pm 0.3) \times 10^{-10}$ $cm^3$ $molecule^{-1}$ $s^{-1})e^{-(2150\pm100)/T}$ over the temperature range 293−623 K. The resulting cyclopropyl radical reacts with molecular chlorine to give chlorocyclopropane. Chlorocyclopropane is approximately a factor of 10 times more reactive than cyclopropane toward chlorine atoms at 296 K and is converted into dichlorocyclopropane. The conclusions drawn from the electronic structure calculations and comparisons with experimental vibrational spectra show that chlorination of chlorocyclopropane predominately leads to the *gem*-dichlorocyclopropane isomer, which inevitably leads to the *gem*-trichlorocyclopropane isomer. The *gem*-$C_3H_4Cl_2$ isomer is both the kinetically and thermodynamically favored product. Chlorination of *gem*-$C_3H_4Cl_2$ can only lead to the *gem*-trichlorocyclopropane isomer.

**Acknowledgment.** The work at Sandia National Laboratories (C.A.T. and J.D.D.) is supported by the Division of Chemical Sciences, Geosciences, and Biosciences, the Office of Basic Energy Sciences, the U. S. Department of Energy. Sandia is a multiprogram laboratory operated by Sandia Corporation, a Lockheed Martin Company, for the United States Department of Energy under Contract DE-AC04-94-AL85000.

## References and Notes

(1) Miller, J. A. *Proc. Combust. Inst.* **2000**, *26*, 461.
(2) Westbrook, C. K. *Proc. Combust. Inst.* **2000**, *28*, 1563.
(3) DeSain, J. D.; Klippenstein, S. J.; Taatjes, C. A.; Hurley, M. D.; Wallington, T. J. *J. Phys. Chem A* **2002**, *107*, 1992.
(4) Wallington, T. J.; Japar, S. M. *J. Atmos. Chem.* **1989**, *9*, 399.
(5) Rice, J. E.; Horn, H.; Lengsfield, B. H.; McLean, A. D.; Carter, J. T.; Replogle, E. S.; Barnes, L. A.; Maluendes, S. A.; Lie, G. C.; Gutowski, M.; Rudge, W. E.; Sauer, S. P. A.; Lindh, R.; Andersson, K.; Chevalier, T. S.; Widmark, P.-O.; Bouzida, D.; Pacansky, G.; Singh, K.; Gillan, C. J.; Carnevali, P.; Swope, W. C.; Liu, B. *Mulliken: A Computational Quantum Chemistry Program*, 2.0 ed.; Almaden Research Center, IBM Research Division: San Jose, CA, 1996.
(6) Dobbs, K. D.; Dixon, D. A. *J. Phys. Chem.* **1994**, *98*, 12584.
(7) Barone, V.; Subra, R. *J. Chem. Phys.* **1996**, *104*, 2630.
(8) Schneider, W. F.; Wallington, T. J.; Barker, J. R.; Stahlberg, E. A. *Ber. Bunsen-Ges. Phys. Chem.* **1998**, *102*, 1850.
(9) Chuang, Y.; Coitiño, E. L.; Truhlar, D. G. *J. Phys. Chem. A* **2000**, *104*, 446.
(10) Johnson, B. G.; Gonzales, C. A.; Gill, P. M. W.; Pople, J. A. *Chem. Phys. Lett.* **1994**, *221*, 100.
(11) Schipper, P. R. T.; Gritsenko, O. V.; Baerends, E. J. *J. Chem. Phys.* **1999**, *111*, 4056.
(12) Scott, A. P.; Radom, L. *J. Phys. Chem.* **1996**, *100*, 16502.
(13) Pilgrim, J. S.; McIlroy, A.; Taatjes, C. A. *J. Phys. Chem. A* **1997**, *101*, 1873.
(14) Farrell, J. T.; Taatjes, C. A. *J. Phys. Chem. A* **1998**, *102*, 4846.
(15) Pilgrim, J. S.; Jennings, R. T.; Taatjes, C. A. *Rev. Sci. Instrum.* **1997**, *68*, 1875.
(16) Atkinson, R. *Chem. Rev.* **1986**, *86*, 69.

(17) DeMore, W. B.; Sander, S. P.; Golden, D. M.; Hampson, R. F.; Kurylo, M. J.; Howard, C. J.; Ravishankara, A. R.; Kolb, C. E.; Molina, M. J. JPL Publication No. 94-26; NASA Jet Propulsion Lab.: Pasadena, CA, 1997.

(18) Baghal-Vayjooee, M.; Benson, S. W. *J. Am. Chem. Soc*. **1979**, *101*, 2838.

(19) Knox, J. H.; Nelson, R. L. *Trans. Faraday Soc*. **1959**, *55*, 937.

(20) Taatjes, C. A.; Christensen, L.; Hurley, M. D.; Wallington, T. J. *J. Phys. Chem. A* **1999**, *103*, 9805.

(21) Donaghy, T.; Shanahan, I.; Hande, M.; Fitzpatrick, S. *Int. J. Chem. Kinet.* **1993**, *25*, 273.

(22) Kaiser, E. W.; Wallington, T. J. *J. Phys. Chem.* **1996**, *100*, 9788.

(23) Pilgrim, J. S.; Taatjes, C. A. *J. Phys. Chem. A* **1997**, *101*, 5776.

(24) Wallington, T. J.; Skewes, L. M.; Siegl, W. O.; Wu, C.-H.; Japar, S. M. *Int. J. Chem. Kinet.* **1988**, *20*, 867.

(25) Nelson, L.; Rattigan, O.; Neavyn, R.; Sidebottom, H.; Treacy, J.; Nielsen, O. J. *Int. J. Chem. Kinet.* **1990**, *22*, 1111.

(26) Cheema, S. A.; Holbrook, K. A.; Oldershaw, G. A.; Walker, R. W. *Int. J. Chem. Kinet.* **2002**, *34*, 110.

(27) Wallington, T. J.; Skewes, L. M.; Siegl, W. O. *J. Phys. Chem*. **1989**, *93*, 3649.

(28) Tyndall, G. S.; Orlando, J. J.; Wallington, T. J.; Dill, M.; Kaiser, E. W. *Int. J. Chem. Kinet.* **1997**, *29*, 43.

(29) Meagher, R. J.; McIntosh, M. E.; Hurley, M. D.; Wallington, T. J. *Int. J. Chem. Kinet*. **1997**, *29*, 619.

(30) (a) Schaefer, H. F., III. In *Atom-Molecule Collision Theory*; Bernstein, R. B., Ed.; Plenum: New York, 1979; p 45. (b) Sosa, C.; Schlegel, H. B. *Int. J. Quantum Chem*. **1986**, *29*, 1001. (c) Sosa, C.; Schlegel, H. B. *Int. J. Quantum Chem*. **1987**, *21*, 267. (d) Gonzalez, C.; Sosa, C.; Schlegel, H. B. *J. Phys. Chem.* **1989**, *93*, 2435.

(31) Steinfeld, J. I.; Francisco, J. S.; Hase, W. L. *Chemical Kinetics and Dynamics*; Prentice Hall, Upper Saddle River, New Jersey, 1989.

(32) Hehre, W. J.; Ditchfield, R.; Radom, L.; Pople, J. A. *J. Am. Chem. Soc*. **1970**, *92*, 4796.

(33) Hehre, W. J.; Radom, L.; Schleyer, P. v. R.; Pople, J. A. *Ab Initio Molecular Orbital Theory*; Wiley: New York, 1986.

(34) Chase, M. W. NIST-JANAF Thermochemical Tables, 4th ed. *J. Phys. Chem. Ref. Data, Monogr. 9* **1998**, 1−1951.

(35) Kerr, J. A.; Smith, A.; Trotman-Dickenson, A. F. *J. Chem. Soc. A* **1969**, 1400.

(36) Walsh, R. *Int. J. Chem. Kinet*. **1970**, *2*, 71.

(37) Arnold, P. A.; Carpenter, B. K. *Chem. Phys. Lett*. **2000**, *90*−*96*, 328.

(38) Mann, D. J.; Hase, W. L. *J. Am. Chem. Soc*. **2002**, *124*, 3208.